Materials Science & Engineering C 108 (2020) 110394

Contents lists available at ScienceDirect

Materials Science & Engineering C

journal homepage: www.elsevier.com/locate/msec

ZnO nanoparticle-incorporated native collagen films with electro-conductive properties

Mireia Andonegi, Miriam Peñalba, Koro de la Caba*, Pedro Guerrero*

BIOMAT Research Group, University of the Basque Country (UPV/EHU), Escuela de Ingeniería de Gipuzkoa, Plaza de Europa 1, 20018 Donostia-San Sebastián, Spain

ARTICLE INFO

Keywords:
Native collagen
ZnO nanoparticles
Semiconductor
Biosensor

ABSTRACT

Collagen obtained from bovine skin was mechanically pre-treated with the aim of preserving the triple helix structure of native collagen. Furthermore, zinc oxide nanoparticles were incorporated into film forming formulations due to their inherent biological properties, which are of great relevance for biomedical applications. All the films showed good mechanical properties with a predominant elastic behavior, as shown by dynamic mechanical analysis (DMA) curves, and collagen films were easy to handle in both dry and wet states. It is worth noting that the integrity in the wet state was achieved without incorporating chemical crosslinkers, in contrast to chemically treated collagen that must be crosslinked chemically due to collagen denaturation after the pre-treatment. As shown by Fourier Transform Infrared (FTIR) spectroscopy analysis, collagen preserved the triple helix structure, although a slight decrease was observed with the increase of zinc oxide nanoparticles (ZnO NPs) content, which slightly increased the equilibrium swelling values and also caused some changes in the denaturation collagen peak observed above 200 °C by Differential Scanning Calorimetry (DSC) measurements. Additionally, collagen films showed good barrier properties, protection again Ultraviolet (UV) light and optimal Water Vapor Permeability (WVP) values (occlusivity) for biomedical purposes such as wound healing, since the WVP values measured would allow exudates' absorption. Regarding electrical conductivity, collagen films presented a semiconductor behavior and memory properties and, thus, these films could be used as biosensors.

1. Introduction

Collagen is the most abundant protein of the extracellular matrix (ECM) in vertebrates, being approximately 30% of body total protein mass [1]. Collagen consists of three parallel polypeptide-alpha chains in a right-handed triple-helical structure, which self-associates to form highly ordered cross-linked fibrils. Those fibrils, in turn, form insoluble fibers providing the extracellular matrix with a high integrity and mechanical tensile strength due to its tight winding triple helix structure [2]. In that way, there are at least 29 collagen types composed of 46 distinct polypeptide chains, constituting the major part of connective tissues, skin, tendons, blood vessels, cornea, cartilages and bones. Collagen type I is the primary collagen in skin (90%) [3] and it has a long history as a natural material for diverse fields, including pharmaceutical, foods, cosmetics and chemical industries [4,5].

In addition to structural roles, collagen also plays functional roles taking part in tissue regulation, growth and repair [6,7]. Due to its remarkable capacity to act as a substrate for cell adhesion and growth, collagen has been considered as a valuable candidate to design resorbable medical devices. Moreover, collagen is largely non-immunogenic and poorly antigenic and thus, biocompatible [8]. Besides, although collagen is resistant to common proteases having a long lifetime, it can be biodegraded in the body by some enzymes of the matrix metalloproteinase (MMP) family, leading to biodegradable collagenous biomaterials [9]. Those collagen structures, physical and biological properties, and its physical versatility to form gels, films, meshes, scaffolds and fibers make collagen an attractive candidate for biomedical applications. Specifically, collagen-based scaffolds are potential biomaterials for wound dressing of burns, pressure sores and leg ulcers, especially for diabetics, because of their ability to accelerate wound repair, inhibit wound contraction, and stimulate epithelium formation [7,10]. Furthermore, during the past decade, collagen-based biomaterials have been used for other biomedical applications, such as 3D cell culture [11], bone and cartilage repair [12,13], vascular and cardiovascular grafts [14], skin substitutes [15], and corneal defects [16]. Additionally, the interest in biocompatible materials sensitive to external stimuli is increasing rapidly due to the improvement caused in the growth of different kind of cells. For example, electrical stimulation

* Corresponding authors at: University of the Basque Country (UPV/EHU), Escuela de Ingeniería de Gipuzkoa, Plaza de Europa 1, 20018 Donostia-San Sebastián, Spain.

E-mail addresses: koro.delacaba@ehu.eus (K. de la Caba), pedromanuel.guerrero@ehu.eus (P. Guerrero).

https://doi.org/10.1016/j.msec.2019.110394
Received 15 September 2019; Received in revised form 1 November 2019; Accepted 2 November 2019
Available online 05 November 2019
0928-4931/

through electro conductive materials can promote bone repair [17], nerve tissue regeneration [18] and cardiac and skeletal muscle tissues [19].

In recent years, metal oxide nanoparticles have reached a special interest in medical applications. In this regard, zinc oxide has been approved as a generally recognized as safe (GRAS) material by the Food and Drug Administration (FDA) [20]. Zinc oxide nanoparticles (ZnO NPs) have been widely used in foods [21], cosmetics [22], and drug delivery systems [23]. In particular, the incorporation of ZnO NPs into biomaterials has been significantly increased in tissue engineering and regenerative medicine due to their biocompatibility, antibacterial, antiseptic and anti-inflammatory activities, in addition to their capacity to enhance cell adhesion and proliferation [1,24]. In this context, the aim of this study was the incorporation of ZnO NPs into collagen formulations to prepare films and investigate the effect of ZnO NPs on physicochemical, thermal, barrier, morphological (XRD, SEM), mechanical, and electrical properties. It is worth noting that this work provides the relation between physicochemical analyses and the viscoelastic and electrical behavior of collagen films, confirming that the reproducibility of the semiconductor behavior, which is of great relevance for biomedical applications, was not compromised by the addition of ZnO NPs.

2. Materials and methods

2.1. Materials

Bovine collagen was supplied by Tenerias Omega. Zinc oxide nanoparticles (ZnO NPs, Ø < 100 nm, specific surface area of 10–25 m^2/g) were supplied by Sigma-Aldrich. Glycerol, used as plasticizer, was provided by OPPAC Products S.A., and acetic acid was obtained from Panreac Quimica S.L.U.

2.2. Preparation of collagen films

Collagen films with different ZnO NPs contents (0, 2, 4, 6 and 8 wt% on collagen dry basis) were prepared by solution casting. Firstly, collagen skins were treated with NaOH 1 M at room temperature for 12 h. Afterwards, these samples were neutralized with phosphate buffer saline (PBS). These samples were designated as native collagen. Native collagen was grinded and freeze-dried in order to facilitate the subsequent processing. Hence, 5 g of collagen, 20 wt% glycerol (on collagen dry basis) and the amount of ZnO NPs required for each formulation were incorporated into 100 mL of 0.5 M acetic acid. The blends were maintained at room temperature under mechanical stirring at 150 rpm for 3 h and then, poured into Petri dishes and left dry at room temperature to obtain the films. Films were designated as 2ZnO, 4ZnO, 6ZnO and 8ZnO as a function of ZnO NPs content. Films without ZnO were considered as control films. All films were conditioned in a climatic chamber (Alava Ingenieros, Spain) at 25 °C and 50% relative humidity before testing.

2.3. Characterization of collagen films

2.3.1. Amino acid composition

Amino acid analysis of native collagen and collagen treated with 0.5 M acetic acid solution under mechanical stirring for 3 h were performed with a Biochrom 30 + amino acid analyzer physiological system (Biochrom, UK).

2.3.2. Fourier transform infrared (FTIR) spectroscopy

FTIR spectra were carried out on a Nicolet Nexus FTIR spectrometer using a Golden Gate (Specac) ATR sampling accessory. A total of 32 scans were performed at 4 cm^{-1} resolution. Measurements were recorded between 4000 and 800 cm^{-1}. All spectra were smoothed using the Savitzky-Golay function. Second-derivative spectra of the amide I region were used at peak position guides for the curve fitting procedure, using OriginPro 9.1 software.

2.3.3. Moisture content (MC) and mass loss (ML)

To determine the MC of films, samples were weighed (w_0) and then dried at 105 °C for 24 h. After that, samples were reweighed (w_1) and MC was calculated by Eq. (1):

$$MC\ (\%) = \frac{w_0 - w_1}{w_0} x\ 100 \quad (1)$$

Mass loss values were calculated using dried specimens (w_1). Samples were immersed into 200 mL of PBS for 5 days and then, samples were reweighed (w_2). Mass loss was calculated by Eq. (2):

$$ML\ (\%) = \frac{w_1 - w_2}{w_1} x\ 100 \quad (2)$$

Measurements were carried out for three specimens of each sample.

2.3.4. Swelling

In order to study the swelling of films, first, rectangular pieces were weighed (w_i) and then, immersed into PBS. Samples were weighed after immersion into PBS for specific times (w_t), until constant values were achieved. The swelling for three specimens of each sample was calculated by Eq. (3):

$$Swelling\ (\%) = \frac{w_t - w_i}{w_t} x\ 100 \quad (3)$$

2.3.5. Differential scanning calorimetry (DSC)

DSC measurements were performed on a Mettler Toledo DSC 822 (Mettler Toledo, Spain). Samples of around 3 mg were subjected to a two heating ramp at a rate of 10 °C/min, under nitrogen atmosphere: firstly, from 25 °C to 125 °C and then, from 25 °C to 250 °C. Sealed aluminum pans were used to prevent mass loss during the experiment.

2.3.6. Dynamic mechanical analysis (DMA)

Thermo-mechanical measurements were performed using a DMA Explexor 100 N, Gabo Qualimeter (JM Toneu, Spain). Experiments were performed in a temperature range from −100 °C to 250 °C at a heating rate of 2 °C/min. The measurements were carried out under tension at a constant frequency of 1 Hz and the strain applied was fixed at 0.05%.

2.3.7. Ultraviolet-visible (UV–vis) spectroscopy

The light-barrier properties of films were determined by measuring their light absorption at wavelengths ranging from 200 nm to 800 nm, using a UV-Jasco spectrophotometer (Model V-630).

2.3.8. Water vapor permeability (WVP)

WVP was determined in a controlled humidity environment chamber PERME™ W3/0120 (Labthink Instruments Co. Ltd., China), according to ASTM E96-00 [25]. Circles of 7.40 cm diameter, with a test area of 33 cm^2, were cut. The setup was subjected to a temperature of 38 °C and a relative humidity of 90%. Water vapor transmission rate (WVTR) was calculated by Eq. (4):

$$WVTR\left(\frac{g}{s\ cm^2}\right) = \frac{G}{t\ x\ A} \quad (4)$$

where G is the change in weight (g), t is time (s), and A is the test area (cm^2). WVP was calculated by Eq. (5):

$$WVP\left(\frac{g}{cm\ s\ Pa}\right) = \frac{WVTR\ x\ L}{\Delta P} \quad (5)$$

where L is the thickness of the test specimen (cm) and ΔP is the partial pressure difference of the water vapor across the film (Pa). WVP was calculated and reported for three specimens of each sample.

2.3.9. Mechanical properties

Tensile strength (TS) and elongation at break (EB) were measured according to ASTM D 638-03 standard [26], using a MTS Insight 10 electromechanical testing system (MTS, Spain). Sheets were cut into dog-bone-shaped samples of 4.75 mm × 22.25 mm and the crosshead rate was -1 mm/min. Measurements were carried out for five specimens of each sample.

2.3.10. Electrical conductivity

Electrical properties of films were analyzed by a Keithley 4200-SCS equipment for semiconductors analysis in a Faraday cage at room temperature. Two point measurements were carried out with a home-built dispositive, performing linear scans from −20 to 20 V in order to obtain intensity vs voltage curves. The films were placed in contact with two copper sheets, adhered in turn to polycarbonate plates; two copper wires, which came up from the copper plates, were put in contact with the electrodes of the equipment to close the electric circuit. The distance between the two electrodes was 2 mm. The dimensions of the samples were 1.0 cm^2 section and 0.25 mm height.

2.3.11. X-ray diffraction (XRD)

XRD was performed with a diffraction unit PANalytical Xpert PRO, operating at 40 kV and 40 mA. The radiation was generated from a Cu-Kα (λ = 1.5418 Å) source. The diffraction data were collected from 2θ values from 2 to 50°, where θ is the angle of incidence of the X-ray bean on the sample.

2.3.12. Scanning electron microscopy (SEM)

A S-4800 scanning electron microscope (Hitachi, Spain) was used. Samples were mounted on a metal stub with double-side adhesive tape and coated under vacuum with gold, using a JEOL fine-coat ion sputter JFC-1100 (Izasa, Spain) in an argon atmosphere, prior to observation. All samples were examined using an accelerating voltage of 10 kV.

2.4. Statistical analysis

In order to determine significant differences between samples, analysis of variance (ANOVA) was done with SPSS software (SPSS Statistic 25). Tukey's test with a statistically significance at the $P < 0.05$ level was considered for multiple comparisons among different systems.

3. Results

3.1. Amino acids composition

In order to identify the amino acids composition in bovine skin native collagen and treated collagen, elemental analysis was performed and the amount of each amino acid residue is shown in Table 1. Glycine is the major amino acid in both collagens, followed by proline and alanine. The content of both proline and hydroxyproline is 22.1% in native collagen and 22.6% in treated collagen. Furthermore, histidine, lysine and hydroxylysine residues were around 3.7% in both collagens, and no cysteine was found indicating that there were no thiol groups present in collagen.

3.2. Physicochemical properties

The interactions among the components of the films and the integrity of collagen structure were assessed by FTIR analysis and FTIR spectra are exhibited in Fig. 1. All the spectra showed the characteristic absorption bands assigned to the peptide bonds in collagen. Specifically, the absorptions related to the amide A, amide I, amide II and amide III bands appeared at 3300, 1634, 1544, and 1238 cm^{-1}, respectively [27]. In particular, amide I contains three major components: a band at 1650 cm^{-1}, associated to the α-helix/random coil conformation, and two bands corresponding to the β-sheet conformation, which appear at 1615–1630 cm^{-1} and 1680–1700 cm^{-1} [28].

Table 1
Amino acid composition of bovine skin native collagen and treated collagen (expressed as residues/1000 residues).

Amino acid	Native collagen	Treated collagen
Aspartic acid	45.3	44.8
Threonine	16.1	15.9
Serine	37.0	36.8
Glutamic acid	72.5	73.0
Glycine	330.9	331.2
Alanine	109.7	108.9
Valine	18.7	17.8
Methionine	6.0	6.2
Isoleucine	10.3	9.8
Leucine	28.8	33.8
Tyrosine	5.7	6.5
Phenylalanine	15.6	15.9
Hydroxylysine	6.7	6.8
Lysine	25.7	26.4
Histidine	4.5	4.3
Arginine	45.4	45.4
Hydroxyproline	98.1	93.6
Proline	122.9	122.8

As shown in Table 2, the addition of ZnO NPs, decreased the content of α- helix conformation. Additionally, the preservation of the integrity of the triple helix structure of collagen was estimated from the absorption ratio between the Amide III band and the band at 1452 cm^{-1} (A_{III}/A_{1452}) [29]. As shown in Table 2, the A_{III}/A_{1452} ratio slightly decreased, indicating that ZnO NPs slightly modified the triple helical structure of collagen.

The moisture content (MC) and the mass loss (ML) of the films were also analyzed and values are shown in Table 3. On the one hand, all films showed low MC values, decreasing ($P < 0.05$) from 2.0 to 0.6% when ZnO NPs content increased. This slight variation in moisture content may be associated with the hydrophobicity of ZnO NPs [30]. On the other hand, mass loss values increased ($P < 0.05$) from 12.9% in control samples to 22.8% in 8ZnO samples.

Considering that one potential application of collagen films can be as wound dressings, swelling tests were carried out and results are shown in Fig. 2. It is worth noting that all samples maintained their structural integrity after immersion in PBS. Swelling increased rapidly in the first 30 min and the equilibrium, around 100% for control sample and around 130% for samples with ZnO NPs, was achieved after 150 min of immersion in PBS.

3.3. Thermal properties

Thermal denaturation of collagen induces modifications in the collagen structure that can be followed by DSC. All samples exhibited two endothermic peaks, as shown in Fig. 3. The first peak, situated around 100 °C, was related to free water release [31]. This peak temperature increased with the addition of ZnO NPs due to the decrease of moisture content [32], as shown in Table 3. The second endothermic peak appeared between 210 and 250 °C and it was associated to the denaturation of collagen [33].

In order to study the effect of ZnO NPs in the viscoelastic behavior of collagen films, DMA was carried out and the temperature dependence of storage modulus (E′) and loss modulus (E″) of collagen films is shown in Fig. 4a. The storage modulus (E′) is generally related to the stored energy, representing the elastic behavior of the material, while the loss modulus (E″) is used to indicate the energy dissipated as heat [34]. The films showed higher E′ values than E″ values, in the whole temperature range, which determined the predominantly elastic character of the films. As the temperature increased, the samples moduli decreased. The moduli decreased slowly until −10 °C and then, they

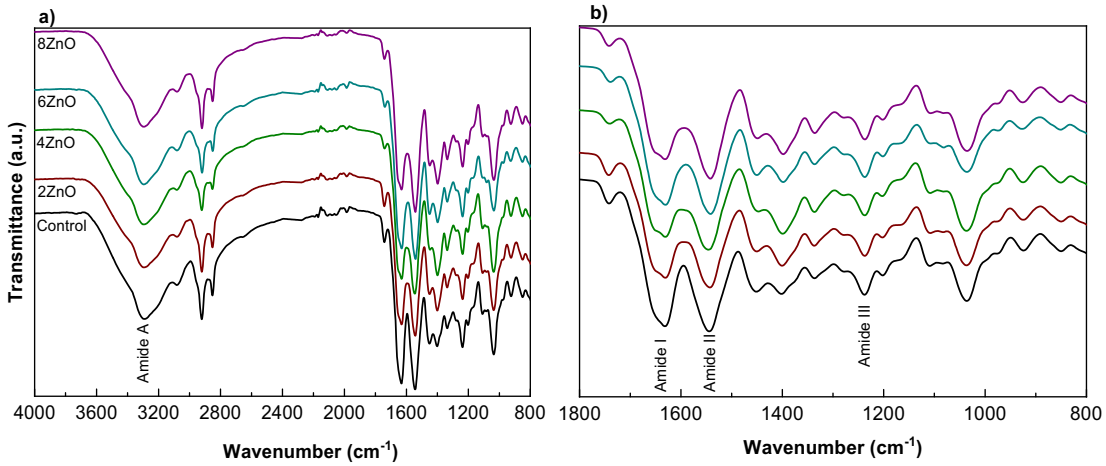

Fig. 1. FTIR spectra of collagen sheets with different ZnO NPs contents: a) from 4000 to 800 cm^{-1} and b) from 1800 to 800 cm^{-1}.

Table 2
Area (%) of the curve fitting of amide I and absorption ratio between amide III band and the band at 1452 cm^{-1} (A_{III}/A_{1452}) for collagen-ZnO NPs films.

Film	β-Sheet (%)	α-Helix/random coil (%)	A_{III}/A_{1452}
Control	36.28	63.72	1.00
2ZnO	36.38	63.62	0.99
4ZnO	38.63	61.37	0.97
6ZnO	40.84	59.16	0.95
8ZnO	42.94	57.06	0.93

Table 3
Moisture content (MC) and mass loss (ML) of collagen-ZnO NPs films.

Film	MC (%)	ML (%)
Control	2.0 ± 0.3[a]	12.9 ± 1.8[a]
2ZnO	1.0 ± 0.1[b]	16.7 ± 1.1[b]
4ZnO	0.9 ± 0.1[bc]	17.3 ± 1.3[b]
6ZnO	0.7 ± 0.1[bc]	22.4 ± 0.9[c]
8ZnO	0.6 ± 0.2[c]	22.8 ± 0.8[c]

[a–c]Two means followed by the same letter in the same column are not significantly ($P > 0.05$) different through the Tukey's multiple range test.

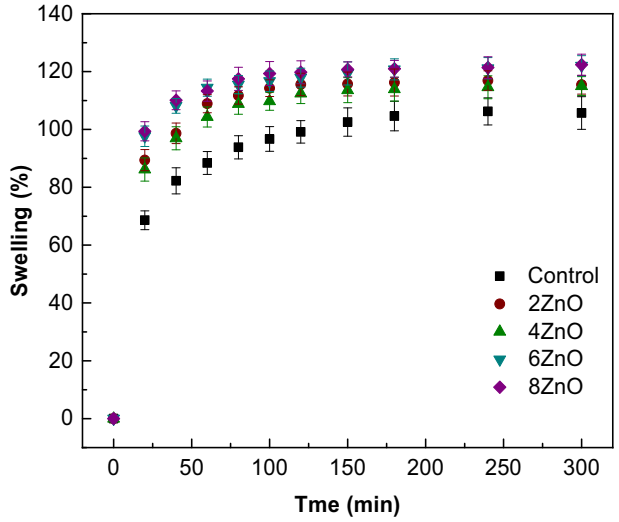

Fig. 2. Swelling curves of collagen films with different ZnO NPs contents.

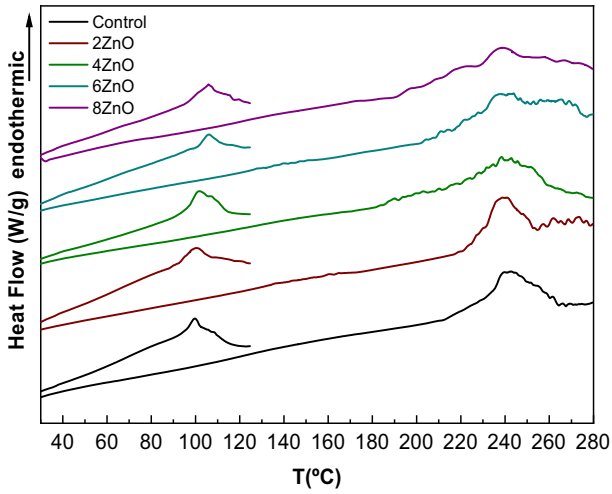

Fig. 3. DSC thermograms of collagen films with different ZnO NPs contents.

dropped sharply up to 20 °C for the control samples and 30 °C for the films with ZnO NPs. This sharp reduction of storage modulus involved the transition of the material from the glassy to the rubbery state [34]. Afterwards, and up to 80 °C, an increase was observed, related to the triple helix structure of collagen.

The loss factor (tan δ), defined as the ratio between loss modulus and storage modulus (tan δ = E″/E′), is represented in Fig. 4b. The temperature at which the loss factor is maximum is defined as the glass transition temperature (T_g). The first glass transition (T_{g1}), at around −60 °C, was attributed to the glass transition of glycerol. The second glass transition (T_{g2}), at around 20 °C for control film and 30 °C for collagen-ZnO NPs films, was attributed to the glass transition of collagen. This increase in T_{g2} could be related to the decrease of films moisture content [32], as shown in Table 3.

3.4. Barrier, mechanical and electrical properties

Light barrier properties were analyzed and UV–vis spectra are shown in Fig. 5. As can be seen, the films exhibited a maximum absorbance peak from 200 to 240 nm, associated with C═O, COOH, $CONH_2$ groups in collagen chains [35,36], and a small absorption peak at 250–280 nm, associated to tyrosine and phenylalanine amino acid residues in collagen [37,38]. The addition of ZnO NPs influenced the films UV–vis absorbance, increasing slightly the absorbance in the visible light range (400–800 nm) and strongly in the UV range, concretely in the 250–280 nm range. Moreover, there was no ZnO NPs

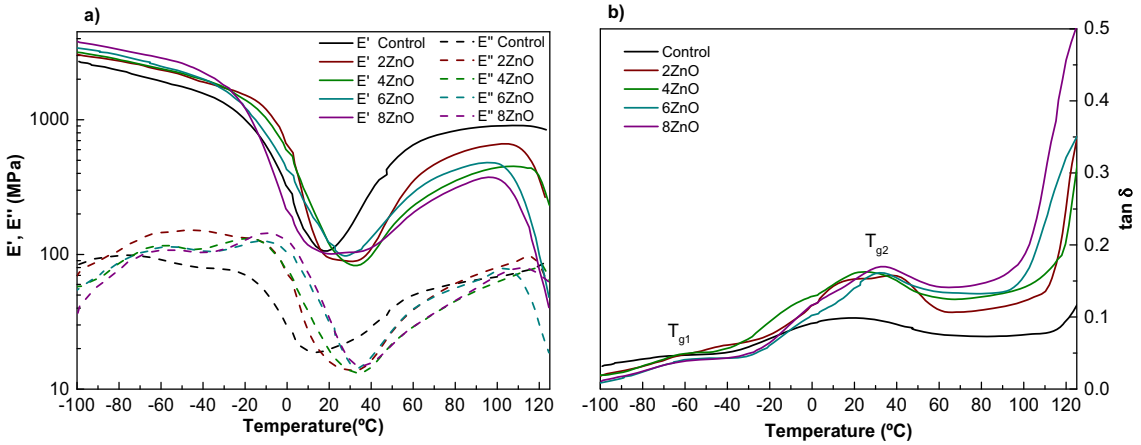

Fig. 4. Temperature dependence of the storage modulus (E′), loss modulus (E″) and loss tangent (tan δ) curves for collagen films with different ZnO NPs contents.

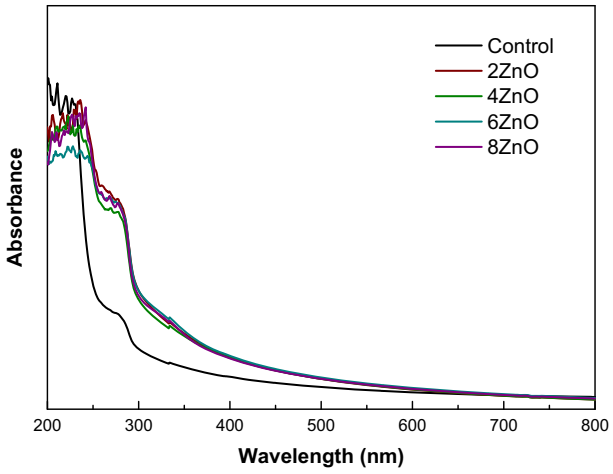

Fig. 5. UV–vis spectra of the collagen films with different ZnO NPs contents.

characteristic absorption peak near 360 nm, suggesting that there were not ZnO NPs with a size larger than the visible wavelength [30].

Concerning water vapor permeability (occlusivity), this is a two-step process: water vapor sorption and water vapor diffusion [39] and it depends on the collagen structure, organization and interactions of collagen molecules in the film [40]. As can be seen in Table 4, there was no difference ($P > 0.05$) with the increase of ZnO NPs content and all samples showed a high occlusive character. In addition to barrier properties, mechanical properties are of great importance to assure that the films are easy to handle. In order to assess the mechanical behavior of collagen films, elastic modulus (EM), tensile strength (TS) and elongation at break (EAB) were measured. As shown in Table 4, EM and TS increased ($P < 0.05$) when ZnO NPs were incorporated into the collagen formulation; however, these values did not change when ZnO NPs increased, as also observed for EAB values.

Table 4
Water vapor permeability (WVP), elastic modulus (EM), tensile strength (TS), and elongation at break (EAB) of collagen films prepared with different ZnO NPs contents.

Films	WVP·10^{12} ($g \cdot cm^{-1} \cdot s^{-1} \cdot Pa^{-1}$)	EM (MPa)	TS (MPa)	EAB (%)
Control	4.9 ± 0.3^{a}	382.8 ± 19.8^{a}	15.9 ± 1.7^{a}	14.4 ± 0.8^{a}
2ZnO	5.6 ± 0.2^{b}	430.7 ± 19.3^{b}	17.7 ± 1.6^{ab}	13.7 ± 0.7^{ab}
4ZnO	5.8 ± 0.4^{b}	445.8 ± 12.3^{b}	18.3 ± 0.7^{b}	13.2 ± 0.2^{b}
6ZnO	5.9 ± 0.4^{b}	452.4 ± 12.1^{b}	18.9 ± 0.4^{b}	13.1 ± 0.5^{b}
8ZnO	5.9 ± 0.6^{b}	455.8 ± 7.2^{b}	19.6 ± 1.3^{b}	12.9 ± 0.6^{b}

$^{a–b}$Two means followed by the same letter in the same column are not significantly ($P > 0.05$) different through the Tukey's multiple range test.

The electrical properties of the films were analyzed from the intensity-voltage (I-V) curves shown in Fig. 6. As can be seen in Fig. 6a, collagen films showed electrical conductivity from negative to positive voltage (blue line) and also from negative to positive voltage (red line). When a positive current passed through the films and operated in the top right quadrant, the curve increased gradually in an extremely small current and voltage. The voltage was swept first from −20 V up to +20 V and then backwards, from +20 V to −20 V. When the forward voltage exceeded 20 V, which was the film internal barrier voltage, avalanche occurred and the forward current increased rapidly for a small increase in voltage producing a non-linear curve, called the "Knee" point. Likewise, when a negative current passed and operated in the bottom left quadrant of the curve, a small gradual decrease of the film electrical resistance was observed, until the reverse voltage across the film became greater than its breakdown voltage point, resulting in a sudden increase in reverse current, producing a fairly straight line downward curve as the voltage losses control. This procedure was repeated several times and Fig. 6b shows the successive sweeps. As can be seen, the initial pinched hysteresis was shifted towards higher currents in the consecutive sweeps, but preserved its shape, illustrating clearly another property of the memristor: memory. Fig. 6b presents the electrical behavior of a collagen film when a current sweep is applied and it shows the reproducibility of the semiconductor electrical behavior. All collagen films showed the characteristic semiconductor electrical behavior and similar resistance values were observed for all films regardless of ZnO NPs contents, as shown in Fig. 6c.

3.5. Morphological properties

In order to determine the film microstructure and relate it to the properties measured, XRD and SEM analyses were carried out. All the films exhibited XRD patterns of amorphous materials (Fig. 7). The peak around 7° indicated the intermolecular lateral packing distance between the molecular collagen chains [41], which is related to the triple helix structure of collagen and, thus, its presence indicated the maintenance of this structure after the addition of ZnO NPs. The broad band centered at 20° is associated to the diffuse scattering of collagen fibers, indicating the amorphous structure of the films. It is worth noting that the characteristic peaks of ZnO at ~31.5°, ~34.4°, and ~36.2° could not be observed due to the interactions between collagen and ZnO NPs, as shown by FTIR analysis.

To further assess the changes caused by the addition of ZnO NPs in the collagen films, SEM analysis was carried out and the images of cross-sections are shown in Fig. 8. SEM micrographs exhibit the dense network of fibers in control films (Fig. 8a). With the addition of ZnO

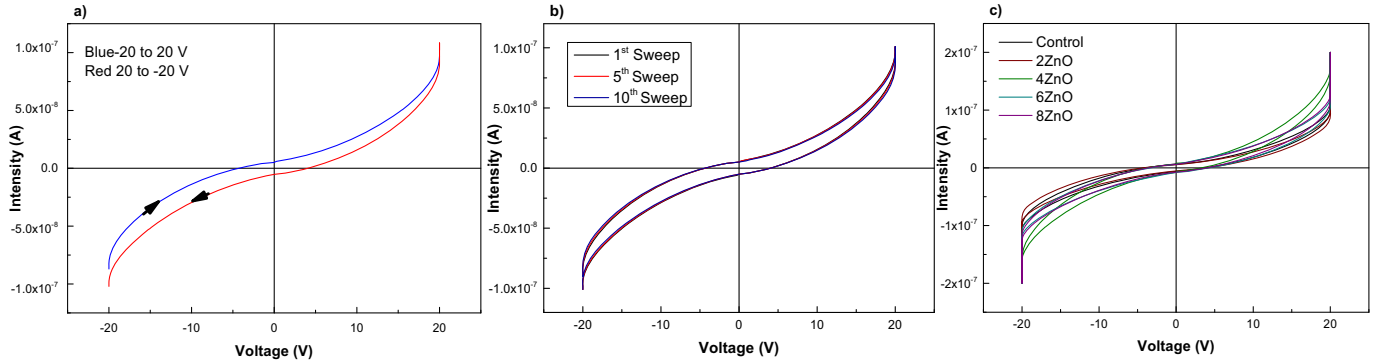

Fig. 6. Intensity-voltage curves of collagen films with different ZnO NPs contents.

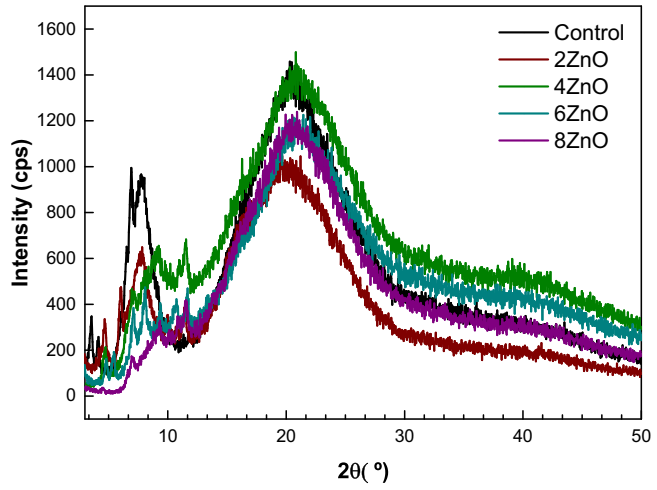

Fig. 7. XRD patterns of collagen films prepared with different ZnO NPs contents.

NPs (Fig. 8b and c) the fibers were not further shown, indicating a structural change to a more compact network, in accordance with the gradual decrease shown in the lateral packaging of collagen chains observed by XRD analysis. Therefore, considering the preservation of the collagen triple helix shown by FTIR results (Table 2), this difference might be related to the decrease of the lateral packing among chains observed by XRD (Fig. 7).

4. Discussion

Amino acid analysis showed that glycine was the most abundant residue in native and treated collagen. Since glycine is the smallest amino acid, its repetition throughout the protein sequence allows close packing of the chains [42]. Furthermore, the high content of both proline and hydroxyproline plays an important role in the structural integrity of collagen, forming hydrogen bonds between collagen α-chains and limiting rotation [43]. Moreover, proline and hydroxyproline contain the pyrrolidine ring, which helps to strengthen the triple helix structure of the collagen [44,45]. Therefore, the amino acid analysis suggests that the stability of the triple helix remains practically intact after the treatment performed. In fact, hydrogen bonding is known to play a significant role in the formation and stabilization of protein secondary structure. In this regard, the amide A band, corresponding to O—H and N—H stretching vibrations, which typically appears at 3400 cm^{-1} in collagen, shifted to 3300 cm^{-1}, indicating hydrogen bonding between collagen, glycerol and ZnO [37,46]. In particular, interpeptide hydrogen bonding stabilizes secondary structures such as the α-helix and β-sheet conformations; therefore, the amide I profile was analyzed with the aim of assessing the effect of ZnO NPs on the secondary structure of collagen. The decrease of α- helix conformation with the addition of ZnO NPs indicated that the protein structure changed as a result of ZnO NPs-collagen interactions. This fact was corroborated by the slight decrease of A_{III}/A_{1452} ratio. FTIR analysis (Fig. 1) also indicated that the interactions among glycerol and collagen occurred by hydrogen bonding, so the mass loss can be attributed to the partial dissolution of glycerol. Moreover, the increase in mass loss values can be associated with the slight loss of the triple helix structure, as shown by A_{III}/A_{1450} ratio (Table 2), which would allow an easier diffusion of glycerol into PBS. In accordance with FTIR and ML results, swelling behavior suggested the existence of physical interactions between ZnO NPs and collagen, which would increase the space between collagen chains and facilitate the film swelling. Collagen films showed the characteristic properties of hydrogels, allowing the permeation of bioactive compounds into the system effectively.

The changes in the triple helix structure shown by FTIR results (Table 2) can be also related to the changes observed by DSC analysis. In this regard, the denaturation peak of collagen, associated to the conformational changes from a triple helix to a random coil structure, changed with the addition of ZnO NPs, specifically, the height of this denaturation peak decreased and its width increased. Furthermore, the intermolecular interactions between collagen and ZnO NPs influenced the viscoelastic behavior of collagen films. As observed by DMA experiments, the temperature at which the minimum values of storage and loss moduli were achieved increased with the addition of ZnO NPs as a consequence of those interactions. Additionally, the subsequent increase of storage and loss moduli after the achievement of the minimum value was smaller for 6ZnO and 8ZnO films, in accordance with the decrease in the content of triple helix structure shown by FTIR results (Table 2).

Considering wound dressing as one feasible application of these collagen-ZnO NPs films, barrier properties are of great importance. Regarding UV barrier properties, the addition of ZnO NPs increased the UV absorbance, concretely in the 250–280 nm range. It is worth noting that collagen films with ZnO NPs showed a strong UV blocking capacity without sacrificing transparency. In order to assess if collagen films could maintain an acceptable level of moisture in the wound when applied as wound dressings, the occlusivity of the films was evaluated measuring water vapor permeability. In this regard, the WVP of collagen films was within the range of commercial wound dressings. Thus, they presented an adequate control of moisture, allowing exudate to evaporate, while maintaining some moisture into the wound to prevent tissue dehydration and help in re-epithelisation.

Considering the special attention acquired by electro conductive biocompatible materials for tissue engineering applications, the electrical properties of the films were analyzed. It is well known that the electrical conductivity of proteins increases enormously with increasing content of adsorbed water, but the conductivity of both wet protein and dry proteins is almost purely electronic. The adsorbed water decreases the semiconduction activation energy, which is lower than 3.0 eV, but

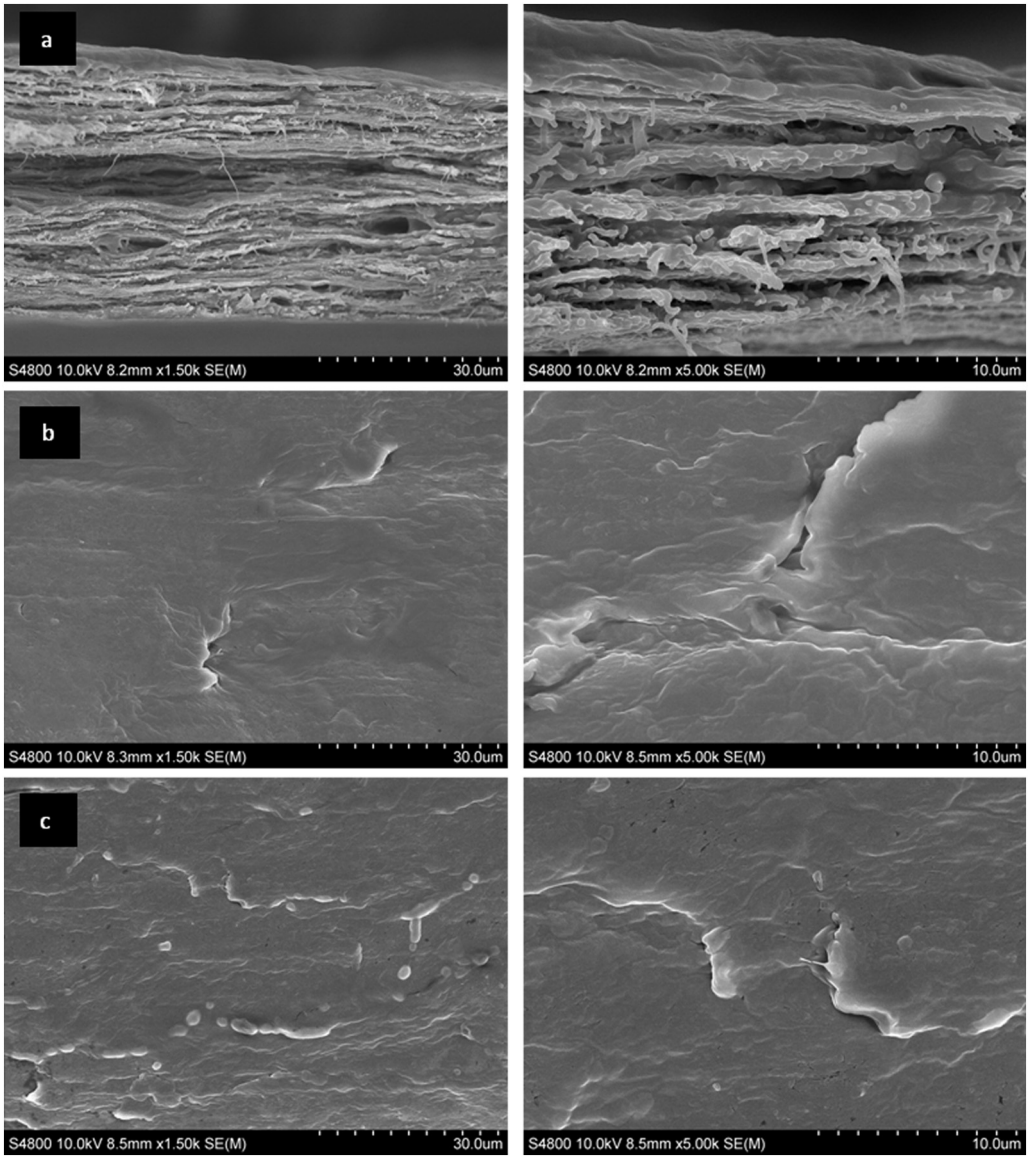

Fig. 8. SEM images of the cross-sections for a) control, b) 4ZnO, and c) 8ZnO films.

does not change the number of states available for releasing mobile charge or the mobility of the charge carriers [47]. From the analysis of intensity voltage (I-V) curves, it can be said that collagen film array behaved like a memristor because the I-V dependence in the range from −20 V to +20 V was strongly nonlinear and showed a pinched hysteretic shape. Collagen films showed the characteristic semiconductor electrical behavior, and the addition of ZnO NPs did not affect the films electrical resistance. Furthermore, the reproducibility of the semiconductor electrical behavior was corroborated by subjecting the films to several electrical sweeps. In addition to the electrical properties of collagen films, tensile tests showed that collagen films were easy to handle and resistant; in particular, tensile strength increased with the addition of ZnO NPs. This mechanical behavior is in accordance with the film microstructure observed by SEM, which showed that the addition of ZnO NPs caused an increase of film compactness. Additionally, all collagen films showed amorphous structure, as observed by XRD analysis, which also showed that the maintenance of the triple helix structure after the addition of ZnO NPs, in accordance with FTIR results (Table 2).

5. Conclusions

Collagen was mechanically pretreated, maintaining its native structure, and subsequently processed to obtain films with induced electro-conductive properties, which could be used to promote cell growth and make these collagen films suitable for biomedical applications. With this in mind, zinc oxide nanoparticles (ZnO NPs) were incorporated into film forming formulations and the effect of ZnO NPs content was assessed. The obtained films showed good mechanical properties and were easy to handle, preserving their physical integrity after immersion into PBS and indicating the maintenance of the triple helix structure, as observed by FTIR analysis and corroborated by XRD results. This fact is of great relevance since the preservation of the triple helix structure allows to avoid the use of chemical crosslinkers, necessary when collagen is chemically treated due to collagen denaturation during the chemical treatment. Furthermore, collagen films showed good occlusivity values for the absorption of fluids, highlighting the potential use of these films as wound dressings. Furthermore, collagen films showed a semiconductor behavior, which was maintained after current sweeps and with the incorporation of ZnO NPs. These induced electro-conductive properties could be used to promote cell growth and

make these collagen films suitable for biomedical applications.

Declaration of competing interest

Authors declare no conflict of interest.

Acknowledgments

Authors thank the Ministry of Science, Innovation and Universities (RTI2018-097100-B-C22), the Basque Government (Department of Quality and Food Industry), and the Provincial Council of Gipuzkoa (Department of Economic Development, the Rural Environment and Territorial Balance) for financial support. Mireia Andonegi thanks the Basque Government (PRE_2017_1_0025) for her fellowship. Thanks also Advanced Research Facilities (SGIker) from the UPV/EHU.

References

[1] P.C. Balaure, A.M. Holban, A.M. Grumezescu, G.D. Mogoşanu, T.A. Bălşeanu, M.S. Stan, A. Dinischiotu, A. Volceanov, L. Mogoantă, *In vitro* and *in vivo* studies of novel fabricated bioactive dressings based on collagen and zinc oxide 3D scaffolds, Int. J. Pharm. 557 (2019) 199–207, https://doi.org/10.1016/j.ijpharm.2018.12.063.

[2] B. An, Y. Lin, B. Brodsky, Collagen interactions: drug design and delivery, Adv. Drug Deliv. Rev. 97 (2016) 69–84, https://doi.org/10.1016/j.addr.2015.11.013.

[3] C. Ding, M. Zhang, G. Li, The response of collagen molecules in acid solution to temperature, Polymer 55 (2014) 5751–5759, https://doi.org/10.1016/j.polymer.2014.09.011.

[4] P.K. Bhagwat, P.B. Dandge, Isolation, characterization and valorizable applications of fish scale collagen in food and agriculture industries, Biocatal. Agric. Biotechnol. 7 (2016) 234–240, https://doi.org/10.1016/j.bcab.2016.06.010.

[5] A. Sorushanova, L.M. Delgado, Z. Wu, N. Shologu, A. Kshirsagar, R. Raghunath, A.M. Mullen, Y. Bayon, A. Pandit, M. Raghunath, D.I. Zeugolis, The collagen suprafamily: from biosynthesis to advanced biomaterial development, Adv. Mater. 31 (2019) 1801651, , https://doi.org/10.1002/adma.201801651.

[6] A.M. Ferreira, P. Gentile, V. Chiono, G. Ciardelli, Collagen for bone tissue regeneration, Acta Biomater. 8 (2012) 3191–3200, https://doi.org/10.1016/j.actbio.2012.06.014.

[7] S.A. Ghodbane, M.G. Dunn, Physical and mechanical properties of cross-linked type I collagen scaffolds derived from bovine, porcine, and ovine tendons, J. Biomed. Mater. Res. Part A 104 (2016) 2685–2692, https://doi.org/10.1002/jbm.a.35813.

[8] A.K. Lynn, I.V. Yannas, W. Bonfield, Antigenicity and immunogenicity of collagen, J. Biomed. Mater. Res. 71B (2004) 343–354, https://doi.org/10.1002/jbm.b.30096.

[9] F. Fu, X. Zhu, Z. Qin, J.J. Wang, C. Xu, L.N. Wang, Y. Tu, S. Zhang, R.X. Li, X.H. Li, M.L. Zhao, Differential degradation rate and underlying mechanism of a collagen/chitosan complex in subcutis, spinal cord and brain tissues of rat, J. Mater. Sci. Mater. Med. 29 (2018) 35, https://doi.org/10.1007/s10856-018-6033-9.

[10] V. Vijayakumar, S.K. Samal, S. Mohanty, S.K. Nayak, Recent advancements in biopolymer and metal nanoparticles-based materials in diabetic wound healing management, Int. J. Biol. Macromol. 122 (2019) 137–148, https://doi.org/10.1016/j.ijbiomac.2018.10.120.

[11] K. Miyazaki, J. Oyanagi, D. Hoshino, S. Togo, H. Kumagai, Y. Miyagi, Cancer cell migration on elongate protrusions of fibroblasts in collagen matrix, Sci. Rep. 9 (2019) 292, https://doi.org/10.1038/s41598-018-36646-z.

[12] B. Liu, F. Yang, X. Wei, X. Zhang, Y. Zhang, B. Wang, G. Liu, H. Xie, J. Yang, W. Wang, K. Qin, D. Zhao, An exploratory study of articular cartilage and subchondral bone reconstruction with bone marrow mesenchymal stem cells combined with porous tantalum/Bio-Gide collagen membrane in osteonecrosis of the femoral head, Mater. Sci. Eng. C 99 (2019) 1123–1132, https://doi.org/10.1016/j.msec.2019.02.072.

[13] W. Yang, Y. Zheng, J. Chen, Q. Zhu, L. Feng, Y. Lan, P. Zhy, S. Tang, R. Guo, Preparation and characterization of the collagen/cellulose nanocrystals/USPIO scaffolds loaded kartogenin for cartilage regeneration, Mater. Sci. Eng. C 99 (2019) 1362–1373, https://doi.org/10.1016/j.msec.2019.02.071.

[14] S. Zouhair, P. Aguiari, L. Iop, A. Vásquez-Rivera, A. Filippi, F. Romanato, S. Korossis, W.F. Wolkers, G. Gerona, Preservation strategies for decellularized pericardial scaffolds for off-the-shelf availability, Acta Biomater. 84 (2019) 208–221, https://doi.org/10.1016/j.actbio.2018.10.026.

[15] X. Liu, C. Zheng, X. Luo, X. Wang, H. Jiang, Recent advances of collagen-based biomaterials: multi-hierarchical structure, modification and biomedical applications, Mater. Sci. Eng. C 99 (2019) 1509–1522, https://doi.org/10.1016/j.msec.2019.02.070.

[16] H. Goodarzi, K. Jadidi, S. Pourmotabed, E. Sharifi, H. Aghamollaei, Preparation and in vitro characterization of cross-linked collagen-gelatin hydrogel using EDC/NHS for corneal tissue engineering applications, Int. J. Biol. Macromol. 126 (2019) 620–632, https://doi.org/10.1016/j.ijbiomac.2018.12.125.

[17] M.R. Kumar, M.S. Freund, Electrically conducting collagen and collagen-mineral composites for current stimulation, RSC Adv. (71) (2015) 57318–57327, https://doi.org/10.1039/c5ra07500a.

[18] Y. Wu, L. Wang, X. Zhao, S. Hou, B. Guo, P.X. Ma, Self-healing supramolecular bioelastomers with shape memory property as a multifunctional platform for biomedical applications *via* modular assembly, Biomaterials 104 (2016) 18–31, https://doi.org/10.1016/j.biomaterials.2016.07.011.

[19] J.O. You, M. Rafat, G.J.C. Ye, D.T. Auguste, Nanoengineering the heart: conductive scaffolds enhance connexin 43 expression, Nano Lett. 11 (2011) 3643–3648, https://doi.org/10.1021/nl201514a.

[20] A. Ullah, I. Zainol, R.H. Idrus, Incorporation of zinc oxide nanoparticles into chitosan-collagen 3D porous scaffolds: effect on morphology, mechanical properties and cytocompatibility of 3D porous scaffolds, Int. J. Biol. Macromol. 104 (2017) 1020–1029, https://doi.org/10.1016/j.ijbiomac.2017.06.080.

[21] G.D. Venkatasubbu, R. Baskar, T. Anusuya, C.A. Seshan, R. Chelliah, Toxicity mechanism of titanium dioxide and zinc oxide nanoparticles against food pathogens, Colloids Surf. B: Biointerfaces 148 (2016) 600–606, https://doi.org/10.1016/j.colsurfb.2016.09.042.

[22] Y. Huang, S.C. Lenaghan, L. Xia, J.N. Burris, C.N. Stewart Jr., M. Zhang, Characterization of physicochemical properties of ivy nanoparticles for cosmetic application, J. Nanobiotechnol. 11 (2013) 3, https://doi.org/10.1186/1477-3155-11-3.

[23] M. Martínez-Carmona, Y. Gun'ko, M. Vallet-Regí, ZnO nanostructures for drug delivery and theranostic applications, Nanomaterials 8 (4) (2018) 268, https://doi.org/10.3390/nano8040268.

[24] K.R. Soumya, S. Snigdha, S. Sugathan, J. Mathew, E.K. Radhakrishnan, Zinc oxide-curcumin nanocomposite loaded collagen membrane as an effective material against methicillin-resistant coagulase-negative Staphylococci, 3 Biotech 7 (2017) 238, https://doi.org/10.1007/s13205-017-0861-z.

[25] ASTM E96-00, Standard test methods for water vapour transmission of material, Annual Book of ASTM Standards, American Society for Testing and Materials, Philadelphia, 2000.

[26] ASTM D 638-03, Standard test method for tensile properties of plastics, Annual Book of ASTM Standards, American Society of Testing and Materials, Philadelphia, 2003.

[27] T. Riaz, R. Zeeshan, F. Zarif, K. Ilyas, N. Muhammad, S.Z. Safi, A. Rahima, S.A.A. Rizvi, I.U. Rehman, FTIR analysis of natural and synthetic collagen, Appl. Spectrosc. Rev. 53 (2018) 703–746, https://doi.org/10.1080/05704928.2018.1426595.

[28] A. Etxabide, I. Leceta, S. Cabezudo, P. Guerrero, K. de la Caba, Sustainable fish gelatin films: from food processing waste to compost, ACS Sustain. Chem. Eng. 4 (2016) 4626–4634, https://doi.org/10.1021/acssuschemeng.6b00750.

[29] D. Shi, F. Liu, Z. Yu, B. Chang, H.D. Goff, F. Zhong, Effect of aging treatment on the physicochemical properties of collagen films, Food Hydrocoll. 87 (2019) 436–447, https://doi.org/10.1016/j.foodhyd.2018.08.016.

[30] S. Ni, H. Zhang, P.M. Godwin, H. Dai, H. Xiao, ZnO nanoparticles enhanced hydrophobicity for starch film and paper, Mater. Lett. 230 (2018) 207–210, https://doi.org/10.1016/j.matlet.2018.07.075.

[31] C.A. Miles, M. Gelashvili, Polymer in a box mechanism for the thermal stabilization of collagen molecules in fibers, Biophys. J. 76 (1999) 3243–3252, https://doi.org/10.1016/S006-3495(99)77476-X.

[32] A. Rochdi, L. Foucat, J.P. Renou, Effect of thermal denaturation on water-collagen interactions: NMR relaxation and differential scanning calorimetry analysis, Biopolymers 50 (1999) 690–696, https://doi.org/10.1002/(SICI)1097-0282(199912)50:7<690::AID-BIP2>3.0.CO;2-P.

[33] L. Bozec, M. Odlyha, Thermal denaturation studies of collagen by microthermal analysis and atomic force microscopy, Biophys. J. 101 (2011) 228–236, https://doi.org/10.1016/j.bpj.2011.04.033.

[34] P. Guerrero, A. Muxika, I. Zarandona, K. de la Caba, Crosslinking of chitosan films processed by compression molding, Carbohydr. Polym. 206 (2019) 820–826, https://doi.org/10.1016/j.carbpol.2018.11.064.

[35] G.K. Pal, T. Nidheesh, P.V. Suresh, Comparative study on characteristics and *in vitro* fibril formation ability of acid and pepsin soluble collagen from the skom pf catla (*Catla catla*) and rohu (*Labeo rohita*), Food Res. Int. 76 (2015) 804–812, https://doi.org/10.1016/j.foodres.2015.07.018.

[36] A. Veeruraj, M. Arumugam, T. Balasubramanian, Isolation and characterization of thermostable collagen from marine eel-fish (Evenchelys macrura), Process Biochem. 48 (2013) 1592–1602, https://doi.org/10.1016/j.procbio.2013.07.011.

[37] R. Duan, J. Zhang, X. Du, X. Yao, K. Konno, Properties of collagen from skin, scale and bone of carp (Cyprinus carpio), Food Chem. 112 (2009) 702–706, https://doi.org/10.1016/j.foodchem.2008.06.020.

[38] Y.R. Huang, C.Y. Shiau, H.H. Chen, B.C. Huang, Isolation and characterization of acid and pepsin-solubilized collagens from the skin of balloon fish (*Diodoon holocanthus*), Food Hydrocoll. 25 (2011) 1507–1513, https://doi.org/10.1016/j.foodhyd.2011.02.011.

[39] J. Uranga, A.I. Puertas, A. Etxabide, M.T. Dueñas, P. Guerrero, K. de la Caba, Citric acid-incorporated fish gelatin/chitosan composite films, Food Hydrocoll. 86 (2019) 95–103, https://doi.org/10.1016/j.foodhyd.2018.02.018.

[40] Y. Ma, W. Wang, Y. Wang, Y. Guo, S. Duan, K. Zhao, S. Li, Metal ions increase mechanical strength and barrier properties of collagen-sodium plyacrilate composite films, Int. J. Biol. Macromol. 119 (2018) 15–22, https://doi.org/10.1016/j.ijbiomac.2018.07.092.

[41] G.A. Valencia, C.G. Luciano, R.V. Lourenço, A.M.Q.B. Bittante, P.J.A. Sobral, Morphological and physical properties of nano-biocomposite films base on collagen loaded with laponite®, Food Packaging Shelf 19 (2019) 24–30, https://doi.org/10.1016/j.fpsl.2018.11.013.

[42] K.A. Piez, Molecular and aggregate structures of the collagens, in: K.A. Piez, A.H. Reddi (Eds.), Extracellular Matrix Biochemistry, Elsevier, New York, 1984, pp. 1–39.

[43] G.N. Ramachandran, Stereochemistry of collagen, Int. J. Pept. Protein Res. 31 (1988) 1–16, https://doi.org/10.1111/j.1399-3011.1988.tb00001.x.
[44] G.K. Pal, P.V. Suresh, Comparative assessment of physicochemical characteristics and fibril formation capacity of thermostable carp scales collagen, Mater. Sci. Eng. C 70 (2017) 32–40, https://doi.org/10.1016/j.msec.2016.08.047.
[45] L.T. Minh Thuy, E. Okazaki, K. Osako, Isolation and characterization of acid-soluble collagen from the scales of marine fishes from Japan and Vietnam, Food Chem. 149 (2014) 264–270, https://doi.org/10.1016/j.foodchem.2013.10.094.
[46] W. Liao, X. Guanghua, Y. Li, X.R. Shen, C. Li, Comparison of characteristics and fibril-forming ability of skin collagen from barramundi (*Lates calcarifer*) and tilapia (*Oreochromis niloticus*), Int. J. Biol. Macromol. 107 (2018) 549–559, https://doi.org/10.1016/j.ijbiomac.2017.09.022.
[47] B. Rosenberg, Electrical conductivity of proteins, Nature 193 (1962) 364–365, https://doi.org/10.1038/193364a0.